Department of Mathematics and Statistics

Preprint MPS-2015-18

30 September 2015

Diagnosing observation error correlations for Doppler radar radial winds in the Met O ce UKV model using observation-minus-background and

to the use of superobservations or the background error covariance matrix used in the assimilation. The large horizontal correlation length scales are, however, in part,

Desroziers et al. [2005]. We describe the DRW observations and their model representations in Section 3 and in Section 4 we describe the experimental design. In Section 5 we consider the estimated observation error statistics from four different cases. Finally we conclude in Section 6.

2 The diagnostic of Desroziers et al. [2005]

Data assimilation techniques combine observations $\mathbf{y} \in \mathbb{R}^{N_p}$ with a model prediction of the state, the background $\mathbf{x}^b \in \mathbb{R}^{N_m}$, often determined by a previous forecast. Here N_p and N_m denote the dimensions of the observation and model state vectors respectively. In the assimilation the observations and background are weighted by their respective errors, using the background and observation error covariance matrices $\mathbf{B} \in \mathbb{R}^{N_m \times N_m}$ and $\mathbf{R} \in \mathbb{R}^{N_p \times N_p}$, to provide a best estimate of the state $\mathbf{x}^a \in \mathbb{R}^{N_m}$, known as the analysis. To calculate the analysis the background must be projected into the observation space using the possibly non-linear observation operator, $H : \mathbb{R}^{N_p} \to \mathbb{R}^{N_m}$

3 Doppler Radar radial wind observations and their model representation

3.1 The Met O ce UKV model and 3D variational assimilation scheme

The operational UKV model is a variable resolution convection permitting model that

et al. [2000], rst interpolates the NWP model horizontal an

of melting ice resulting in intense re ectivity return [Kit

creating the superobservations using the background does not introduce any background error into ^{so}) if:

1. The observation and background errors are independent;
2. The background state errors are fully correlated within the superobservation cell;
3. The background state errors in a superobservation cell have the same magnitude and
4. The background residuals are equally weighted within a superobservation cell.

However, for DRWs it is not clear that all the assumptions will hold. In particular assumptions 1 and 2 are valid at close range to the radar where the superobservation cells are small. However, at far range the superobservation cells are large and the assumptions are likely to be invalid. Therefore, it is possible that at large ranges there is a small influence of the background errors on the error associated with the superobservation.

with the observation operator described in equation (11). We summarise the different cases in Table 1.

Table 1 – Summary of experimental design for different cases

Case	B	Superobservations	Observation Operator
1	New	Yes	Old
2	Old	Yes	Old
3	New	No	Old
4	New	No	New

For each case the available data for each radar scan is stored in 3D arrays of size $N^s \times N^r \times N^a$ where N^s is the number of scans containing data, $N^r = 16$ is the number of ranges and $N^a = 120$ is the number of azimuths. Figure 1 shows a radar scan with the typical superobservation cells. The data is also separated by elevation, with data available at elevation angles of 1^o, 2^o, 4^o and 6^o. (We do not estimate the observation error statistics for the 9^o beam due the lack of avaliable data). The position of these observations at these elevations are shown in Figure 2, we note that the color scheme for each given elevation is used throughout the figures in this manuscript. It is important to note that these observations are only available in areas where there is precipitation and it is possible that only part of the scan contains observations. Furthermore, the use of the superobservations, thinning and quality control results in a limited amount of data in each scan. The amount of data available differs for each elevation, with data for the lower elevations available at far range, and for higher elevations available for near range. This lack of data means that standard deviations and correlations are not available for every range at each elevation. Results are not plotted for standard deviations unless 150 samples were available; for correlations the required number of samples is 500. Observations may be correlated along the beam, horizontally or vertically. Here we consider both horizontal correlations and those along the beam.

Horizontal correlations consider how observations at a given height are correlated. The blue cells in Figure 1 show a set of observations that would be compared for a given height. For each radar scan, data is sorted into 200m height bins. Here the height takes into account the height of the radar ab[illegible]

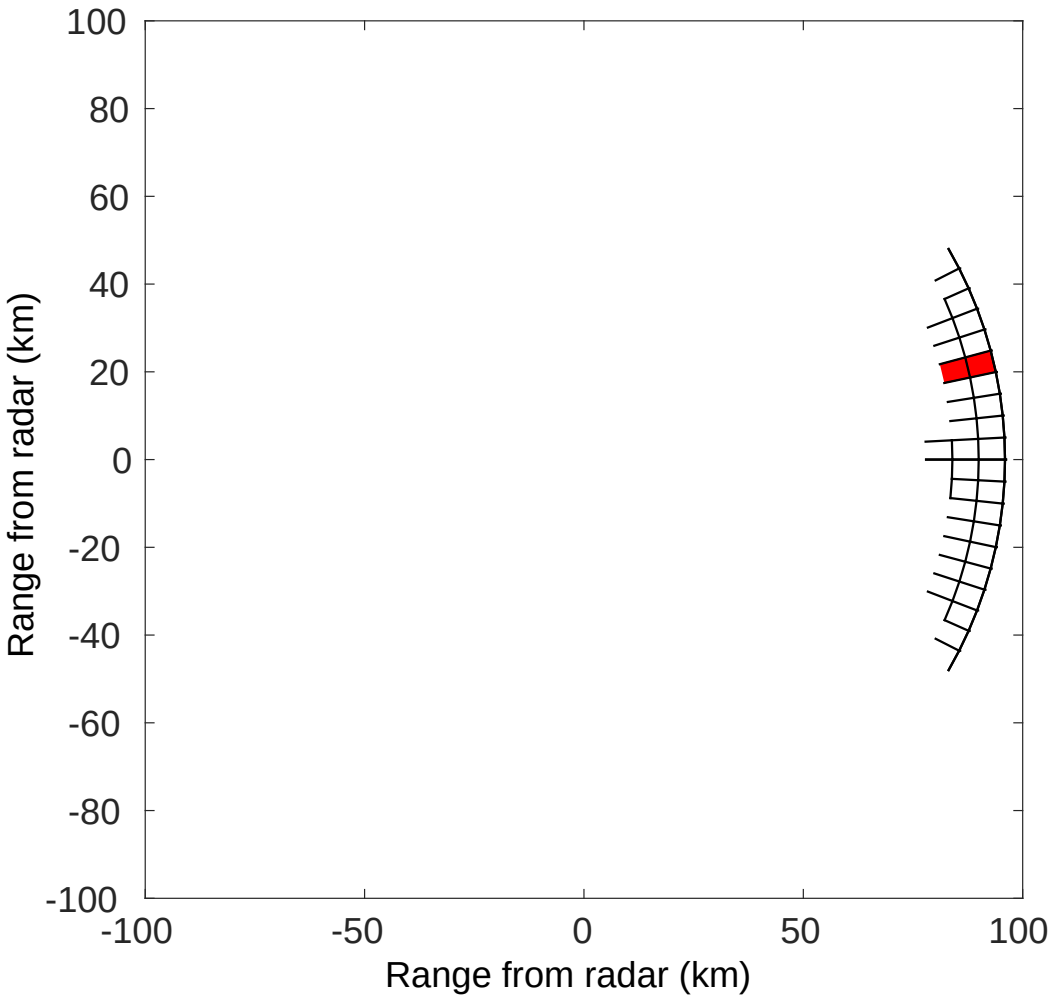
100
80
60
40
20
0
-20
-40
-60
-80
-100
Range from radar (km)
-100
-50
0
50
100
Range from radar (km)

the observation located at 30km range, the correlation with the 18km observation (-12km separation) will have a smaller measurement volume whereas the observation at 42km

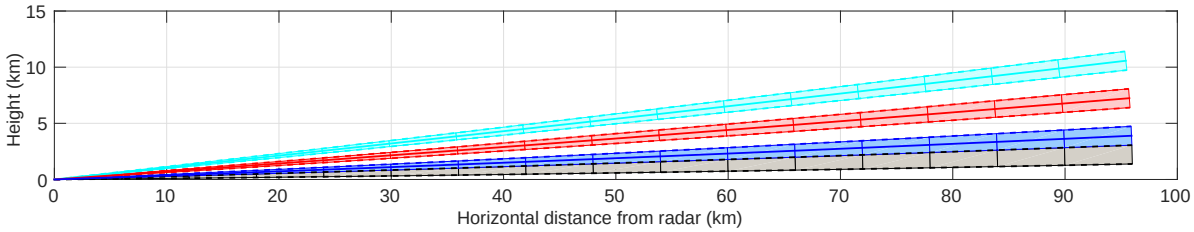
15
10
5
0
Height (km)
0
10
20
30
40
50
60
70
80
90
100
Horizontal distance from radar (km)

It is also possible to compare observations at the same range, gate, observations will have the same measurement volume but will be at different heights in the atmosphere. In this case we find that for each elevation the correlation length scales are similar, e.g. at a range of 40km each elevation has a correlation length scale of 23km (not shown). This suggests that the the measurement volume of the observation has the largest impact on the horizontal correlation length scale, with correlation length scale increasing with measurement volume.

5.1.2 Along-beam correlations

Next we calculate the along-beam observation errors using the data from Case 1. We begin

reassuring and suggest that we are obtaining a reasonable estimate of the observation error correlations.

Next we calculate the error statistics along the beam for each elevation. In Figure 8 (square symbols) we plot the change in standard deviation with height for beam elevations 1°, 2°, 4° and 6°. (For the horizontal correlations the height of the radar above sea level was

angles have larger beam gradients, di erent gates sample a wider range of heights in the atmosphere; this results in small observation error correlations.

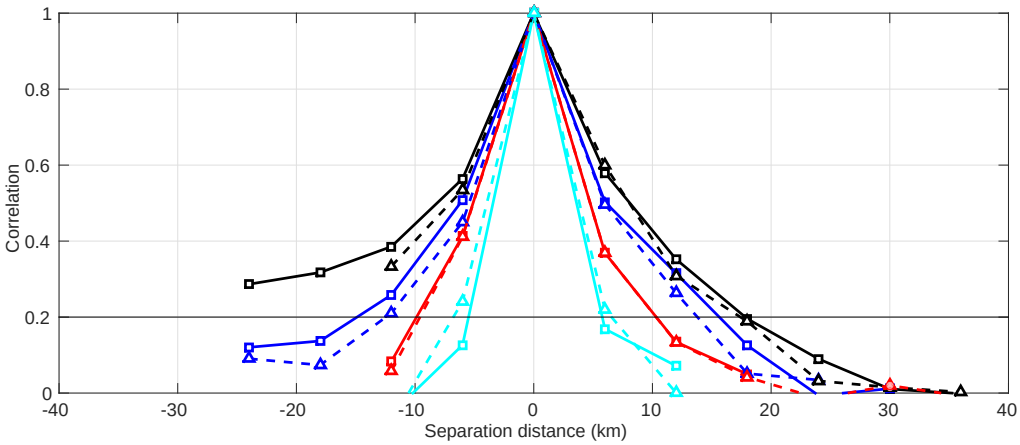

Figure 11 { Correlations along the beam at range 40km for elevations and approximate heights 1^o 0:8km (black), 2^o 1:5km (blue), 4^o 3:0km (red) and , 6^o 4:3km (cyan) for superobbed data (solid lines) and thinned raw data (dashed lines). Error correlations are deemed to be insigni cant below the horizontal line at 0.2.

5.1.3 Summary

For this case we have calculated observation error statistics using data from the January 2014 operational UKV KV onal UKo

When considering the standard deviations for each elevation we again see that they are reduced (see diamonds Figure 8). Though the change in standa

observation error correlation length scales for observations that are at lower elevations

Using thinned raw data has little impact on the estimated observation error standard

5.4.2 Along-beam correlations

In this case Table 2 and Figure 8 show that the error standard deviation is reduced compared to Case 3 suggesting that the more sophisticated observation operator is indeed an improved map from background to observation space. Both Fig

horizontally, vertically or along the path of the radar beam. In this work we consider both the horizontal and along-beam error statistics.

Initially error statistics were calculated for observations assimilated into the UKV model operational in January 2014. This provided information on the general structure of the observation errors and how they vary throughout the atmosphere. Error statistics were also calculated using data from an assimilation run using alternative background error statistics. This provided information on how sensitivity of the results to the specification of the background error statistics. The diagnostic was then applied to data from a further two assimilation runs. These evaluated the impact that the use of superobservations and errors in the observation operator have on the estimated observation error statistics.

Results from all four cases showed similar behaviour for the estimated statistics. We are able to conclude that most DRW error standard deviations, horizontal and along-beam correlation length scales increase with height, as a function of the increase in measurement volume. Thus at least part of the correlated errors are likely to be related to the uncertainty in the observation operator. The exceptions are the standard deviations at the lowest heights. Observations at the lowest heights have the smallest measurement volumes, smaller than the model grid spacing, and hence representativity errors may well account for the larger standard deviations at lower heights.

Results showed that the estimated standard deviations are similar those used operationally. However for the majority of cases, with exception of the 6° beam, the correlation length scales are much larger than those found in Simonin et al. [2014] and the operational thinning distance of 6km. Despite the differences in operational system, our estimated average along-beam correlations are similar to those calculated by Météo-France [Wattrelot et al., 2012]. Furthermore, observation error statistics estimated when using an alternative background error covariance matrix in the assimilation and the results from Waller et al. [2015] imply that the observation error correlation length scale is underestimated. This suggests that the errors are correlated to a degree that it should be accounted for in the assimilation.

In an attempt to understand the source of the error correlations, the effect of using superobservations and an improved observation operator are considered. The use of the superobservations does not affect the error standard deviations. However, results suggest that the use of superobservations introduces correlated error at far range, possibly as a result of an invalid assumption in the superobservation calculation. The use of an improved observation operator reduces the error standard deviations, particularly at low elevations and at far range where observations have large measurement volumes. This is expected since the new observation operator takes into account the beam broadening and bending, both of which affect the beam most at far range. The improvement in the low elevations is related to the inclusion in the observation operator of information from more model levels. These are denser in the lower atmosphere where the low elevations provide observations. The use of the new observation operator results in an increase of the along-beam correlation length scale. We hypothesize that this is a result of nearby observation residuals now sharing information from the same model levels. However, the horizontal correlations were

slightly reduced. This suggests not only that some of the horizontal correlations previously seen were a result of omissions in the observation operator, but also that the horizontal correlation length scale may be further reduced with the use of on even more complex observation operator.

These results provide a better understanding of DRW observation error statistics and the sources that contribute to them. We have shown that these observation errors exhibit large spatial correlations that are much larger that the operational thinning distance. This implies that either the data must be thinned further to ensure the errors are uncorrelated or the correlated errors must be accounted for in the assimilation.

Acknowledgments

This work is funded in part by the NERC Flooding from Intense Rainfall programme and the NERC National Centre for Earth Observation.

References

S. Ballard, Z. Li, D. Simonin, and J.-F. Caron. Performance of 4D-Var NWP-based nowcasting of precipitation at the Met Office for summer 2012. Submitted to Quarterly Journal of the Royal Meteorological Society, 2015.

H. Berger and M. Forsythe. Satellite wind superobbing. Technical report, Met Office, UK, 2004. Forecasting Research Technical Report 451.

V. Bondarenko, T. Ochotta, and D. Saupe. The interaction between model resolution, observation resolution and observations density in data assimilation: A two-dimensional study.

S. L. Dance. Issues in high resolution limited area data assimilation for quantitative precipitation forecasting. Physica D: Nonlinear Phenomena, 196:1 { 27, 2004.

D. P. Dee and A. M. Da Silva. Maximum-likelihood estimation of forecast and observation error covariance parameters. Part I: Methodology. Monthly Weather Review, 127:1822{1843, 1999.

G. Desroziers, L. Berre, B. Chapnik, and P. Poli. Diagnosis of observation, background and analysis-error statistics in observation space. Quarterly Journal of the Royal Meteorological Society, 131:3385{3396, 2005.

R. J. Doviak and D. S. Zrnic. Doppler Radar and Weather Observations. Academic Press, second edition, 1993.

F. Fabry. Radial velocity measurement simmulations: common errors, approimations, or ommissions and their impact on estimation accuracy. In Proceedings of of the sixth European conference on radar in meteorology and hydrology, 2010.

S. B. Healy and A. A. White. Use of discrete Fourier transforms in the 1D-Var retrieval problem. Quarterly Journal of the Royal Meteorological Society, 131:63{72, 2005.

A. Hollingsworth and P. Lönnberg. The statistical structure of short-range forecast errors as determined from radiosonde data. Part I: The wind field. Tellus, 38A:111{136, 1986.

T. Janjic and S. E. Cohn. Treatment of observation error due to unresolved scales in atmospheric data assimilation. Monthly Weather Review, 134:2900{2915, 2006.

M. Kitchen. Towards improved radar estimates of surface precipitation rate at long range. Quarterly Journal of the Royal Meteorological Society, 123:145163, 1997.

H. Lean, P. Clark, M. Dixon, N. Roberts, A. Fitch, R. Forbes, and C. Halliwell. Characteristics of high-resolution versions of the Met Office Unified Model for forecasting convection over the United Kingdom. Monthly Waether Review, 136:3408{3424, 2008.

Z. Li, S. Ballard, and D. Simonin. Comparison of 3D-Var and 4D-Var data assimilation in an NWP-based nowcasting system of precipitation at the Met Office. Quarterly Journal of the Royal Meteorological Society, 2015.

M. Lindskog, H. Jarvinen, and D. B. Michelson. Assimilation of radar radial winds in the HIRLAM 3D-Var. Physics and Chemistry of the Earth - Part B: Hydrology, Ocean and Atmosphere, 25:1243{1249, 2000.

M. Lindskog, N. Gustafsson, B. Navascues, K. S. Mogensen, X. Huang, X. Yang, U. Andrae, L. Berre, S. Thorsteinsson, and J. Rantakokko. Three-dimensional variational data assimilation for a limited area model. Part II: Observation handling and assimilation experiments. Tellus, 53A:447{468, 2001.

M. Lindskog, K. Salonen, H. Jaarvinen, and D. B. Michelson. Doppler radar wind assimilation with HIRLAM 3DVAR. Monthly Weather Review, 132:1081{1092, 2004.

Z.-Q. Liu and F. Rabier. The interaction between model resolution observation resolution and observation density in data assimilation: A one dimensional study. Quarterly Journal of the Royal Meteorological Society, 128:1367{1386, 2002.

A. C. Lorenc, S. P. Ballard, R. S. Bell, N. B. Ingleby, P. L. F. Andrews, D. M. Barker, J. R. Bray, A. M. Clayton, T. Dalby, D. Li, T. J. Payne, and F. W. Saunders. The met. o ce global three-dimensional variational data assimilation scheme. Quarterly Journal of the Royal Meteorological Society, 126:2991{3012, 2000.

T. Montmerle and C. Faccani. Mesoscale assimilation of radial velocities from Doppler radars in a preoperational framework. Monthly Weather Review, 137:1939{1953, 2009.

S. K. Park and D. Zupanski. Four-dimensional variational data assimilation for mesoscale and storm-scale applications. Meteorology and Atmospheric Physics

K. Salonen, H. Jarvinen, S. Jarvenoja, S. Niemela, and R. Eresmaa. Doppler radar radial wind data in nwp model validation. Meteorological Applications, 15:97{102, 2008.

K. Salonen, H. Jarvinen, G. Haase, S. Niemela, and R. Eresmaa. Doppler radar radial winds in HIRLAM. Part II: Optimizing the super-observation processing. Tellus, 61A: 288{295, 2009.

D. Simonin. New implementation for the assimilation of Doppler radial wind observations. Technical report, Met O ce, UK, 2014. Progress Report.

D. Simonin, S. Ballard, Z. Li, and J. F. Caron. Doppler radar assimilation. ERAD 201 27th European Conference on Radar in Meteorology and Hydrology, June 2012. http://www.meteo.fr/cic/meetings/2012/ERAD/presenta tions/friday/14-2.pdf.

D. Simonin, S. P. Ballard, and Z. Li. Doppler radar radial wind assimilation using an hourly cycling 3D-Var with a 1.5 km resolution version of the Met O ce Uni ed Model for nowcastings. Quarterly Journal of the Royal Meteorological Society, 2014. doi: 10.1002/qj.2298.

L. M. Stewart. Correlated observation errors in data assimilation. PhD thesis, University of Reading, 2010. http://www.reading.ac.uk/maths-and-stats/research/theses/maths-phdtheses.aspx.

L. M. Stewart, S. L. Dance, and N. K. Nichols. Correlated observation errors in data assimilation. International Journal for Numerical Methods in Fluids, 56:1521{1527, 2008.

L. M. Stewart, J. Cameron, S. L. Dance, S. English, J. R. Eyre, and N. K. Nichols. Observation error correlations in IASI radiance data. Technical report, University of Reading, 2009. Mathematics reports series, www.reading.ac.uk/web/FILES/maths/obs_error_IASI_radiance.pdf.

L. M. Stewart, S. L. Dance, and N. K. Nichols. Data assimilation with correlated observation errors: experiments with a 1-D shallow water model. Tellus A, 65, 2013. doi: http://dx.doi.org/10.3402/tellusa.v65i0.19546.

L. M. Stewart, S. L. Dance, N. K. Nichols, J. R. Eyre, and J. Cameron. Estimating interchannel observation-error correlations for IASI radiance data in the Met O ce system. Quarterly Journal of the Royal Meteorological Society, 140:1236{1244, 2014. doi: 10.1002/qj.2211.

J. Sun. Convective-scale assimilation of radar data: Progresses and challenges. Quarterly Journal of the Royal Meteorological Society, 131:3439{3463, 2005.

J. Sun, M. . Xue, J. W. Wilson, I. Zawadzki, S. P. Ballard, J. Onvlee-Hooimeyer, P. Joe, D. M. Barker, P.-W. Li, B. Golding, M. Xu, and J. Pinto. Use of NWP for nowcasting convective precipitation: Recent progresses and challenges. Bulletin of the American Meteorological Society, 95:409{426, 2014.